Evaluation of the potential of a gamma-ray observatory to detect astrophysical neutrinos

Pedro Valdez Machado de Jesus Costa[1,a]

[1] *Instituto Superior Técnico, Lisbon, Portugal*

Abstract. This thesis aims to determine whether a ground-based gamma-ray observatory is capable of measuring neutrinos with energies ranging from 100 TeV to 1 PeV, and its expected performance. The main objects of study are very inclined extensive air showers induced by down-going and up-going electron neutrinos. Background is predominantly made up of very inclined EAS induced by cosmic-rays. Discrimination between signal and background is based on the balance of the total electromagnetic and total muonic signal on the ground. We demonstrate that a km^2-scale wide-field ground-based gamma-ray observatory is predicted to be capable of detecting VHE atmospheric and astrophysical neutrinos at an average rate of 2.09×10^{-1} yr^{-1}, or ~ 1 event every 5 years. The highest estimated event rate is 3.72×10^{-1} yr^{-1} or ~ 1 event $2-3$ years.

Keywords: Astrophysical Neutrinos; Atmospheric Neutrinos; Gamma-Rays; Cosmic-Rays; Gamma-Ray Ground-Based Observatories

1 Introduction

Astroparticle multi-messenger physics combines information pertaining to a single phenomenon extracted from different messengers, namely electromagnetic radiation, gravitational waves, neutrinos, and cosmic rays. As each messenger is created by different astrophysical processes, they reveal different information about their sources. This approach has the potential to address fundamental problems, such as those related to physics in extreme phenomena, the long-standing question on the origin of UHECRs, the nature of dark matter, the possibility of a Lorentz invariance violation and even the existence of previously undiscovered particles.

There are numerous experiments that resort to EAS detector arrays to study gamma-rays with very-high energies. In this thesis, we use simulation studies to determine whether such experimental setups are capable of neutrino detection, and to estimate the sensitivity that could be expected of them. In particular, our study is restricted to neutrinos with energies ranging from 100 TeV to 1 PeV. Signal events correspond to inclined and very inclined EAS ($\theta > 60°$) induced by down-going and up-going neutrinos. The main source of background for this measurement are very inclined EAS resulting from the interaction of cosmic-rays with the atmosphere. Using the balance between the total electromagnetic signal and total muonic signal registered at the ground level, a cut is introduced to discriminate between neutrino events and cosmic-ray background.

This article opens with a brief introduction to neutrinos, extensive air showers and the current experimental panorama. Secondly, a description the workflow established for the sensitivity computation is provided.This is followed by a discussion of the results pertaining to background elimination and the estimation of the neutrino event rate. Afterwards, the impact of the signal resolution on the proposed measurement is also discussed. Finally, we present the results of the study of the possibility of using up-going neutrinos as an additional contribution to the expected event rate.

[a] e-mail: pedro.j.costa@tecnico.ulisboa.pt

2 Background

2.1 VHE neutrinos

Very-High Energy (VHE; $E_\nu \sim$ PeV) neutrinos may be produced by the decay of secondary particles (such as very energetic muons or charmed particles) originating from the collisions of cosmic rays (typically protons and heavier nuclei) with nuclei in the upper atmosphere. These cases are commonly referred to as atmospheric neutrinos. Given their origin, their flux has a direct correlation with the flux of cosmic rays. For energies below $\sim 100\,\text{TeV} - 1\,\text{PeV}$, the flux of atmospheric neutrinos is the main contributor to the neutrino energy spectrum, as depicted in Figure 1. As the energy increases, the flux of cosmic rays decreases significantly, causing the contribution of atmospheric neutrinos to diminish. At higher energies, the flux of neutrinos originating from astrophysical sources exceeds that of atmospheric neutrinos.

Within astrophysical objects such AGN, the decay of charged pions resulting from the interaction of charged cosmic rays with radiation and/or molecular clouds leads to the production of neutrinos. These VHE and Ultra-High Energy (UHE, $E_\nu \sim$ EeV) particles can travel long distances without being absorbed or deflected by magnetic fields, making them unique tracers of cosmic-ray acceleration that point directly to their sources. For energies exceeding 1 PeV the flux of these neutrinos represents the dominant contribution to the neutrino energy spectrum, as can be seen in Figure 1.

2.2 Extensive Air Showers

When a very energetic particle (the primary particle) enters the atmosphere and interacts with the nucleons of the atoms, new (secondary) particles are produced, among which the energy of the primary particle is divided. In turn, interactions of these particles lead to the production of new particles, a process which is repeated successively, thus generating an extensive air shower which may reach the Earth's surface.

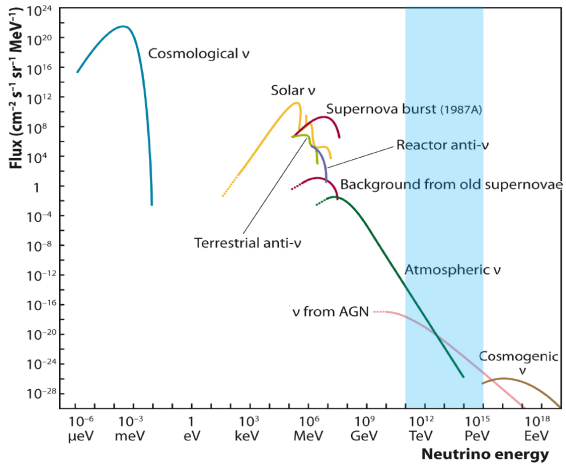

Figure 1: Neutrino energy spectrum, taken from [1]. IceCube focuses on the range of energies 10^{14} – 10^{16} eV, the Pierre Auger Observatory on energies of the order of 10^{18} eV and above, while the SWGO would work in the 10^{11} – 10^{15} eV range, as highlighted in blue.

2.2.1 Neutrino Induced Showers

Vertical neutrino-induced showers and ordinary cosmic-ray-induced showers exhibit very similar signatures, making them hard to distinguish. In the case of inclined and very inclined showers (roughly $\theta > 60°$) this discrimination becomes viable, since there is a larger grammage between the first interaction point and the ground. As a consequence, a proton typically induces a shower long before reaching considerable depths within the atmosphere. This leads to its electromagnetic component being completely absorbed early in its path, thus not reaching the detector array. The end result is a shower front at the ground level that is dominated by muons, which induce sharp time traces in the water Cherenkov stations of an air shower array [2].

In contrast, due to the small interaction cross section of neutrinos, they have a very low probability of interacting with the atmosphere. This means that down-going neutrinos arriving at large zenith angles have the possibility of interacting and developing showers much deeper in the atmosphere, producing traces that spread over longer times [3]. This is the strategy employed by, for instance, the Pierre Auger Observatory to look for neutrino-induced showers [4]. There is also the possibility of showers being induced by up-going neutrinos. Most commonly, this occurs via the Earth-skimming mechanism, which entails a neutrino interacting in the Earth's crust and producing a lepton that then generates a shower [5].

2.2.2 Neutrino Detection

The biggest challenge pertaining to VHE and UHE neutrino detection is increasing the sensitivity of detectors to allow them to see a reasonable number of events, since the flux of neutrinos at these energies is expected to be lower than the photon flux [1].The most common means of addressing this issue is instrumenting very large volumes, typically making use of large amounts of water or ice as is the case of the Baikal Deep Underwater Neutrino Telescope (BDUNT) [6] and the IceCube Neutrino Observatory [7], respectively.

This thesis focuses exclusively on the detection of electron neutrinos. When these particles interact with the atmosphere, they generate an hadronic and an electromagnetic component. The latter constituent is an EM shower induced by the electron produced from the interaction of the corresponding neutrino. Upon reaching the ground, the cascade has undergone a substantial development allowing it to generate a large footprint, facilitating its detection.

The interaction of a tau neutrino or a muon neutrino with the atmosphere also gives rise to an hadronic component. In the case of a muon neutrino, the other product of this interaction is a muon, which can penetrate the atmosphere and reach Earth's surface without generating a particle shower. As a result, very little or no signal is deposited in the array, and no footprint is produced, making detection unfeasible.

In contrast, a tau behaves similarly to a heavier version of the electron, and is more highly penetrating. Due to its mass, it is the only lepton that can decay into hadrons. The possibility of introducing an additional hadronic component means showers induced by tau neutrinos exhibit a more complex and erratic behaviour, although their detection is still viable. Because of this, the simplest case, corresponding to the electron neutrino, was chosen instead.

3 State-of-the-Art

3.1 Astrophysical Neutrino Observatories

There is a wide range of experiments dedicated to the detection of astrophysical neutrinos, such as SNO [8] (now refurbished for use in the SNO+ experiment [9]), Super-Kamiokande [10], ANTARES [11] and the IceCube Neutrino Observatory [7], all of which are water Cherenkov detectors (except for SNO+, which resorts to a liquid scintillator). Neutrino detection can also be achieved via scintillators (e.g.Cowan–Reines neutrino experiment [12] and KamLAND [13]) and radio-chemical methods (e.g. SAGE experiment [14] and GALLEX/GNO experiments [15]). Among the experiments previously mentioned, the IceCube Neutrino Observatory has detected neutrinos with energies of the order of PeV [16] for which jets from GRBs or AGN are possible sources. It also detected neutrinos spatially coincident with the BL Lac-type blazar TXS 0506+056 as it was undergoing a gamma-ray flare [17], an indication that jets accelerate hadrons to very high energies.

The Pierre Auger Observatory is also conducting an experiment that has the potential to detect VHE and UHE astrophysical neutrinos. This observatory makes use of a hybrid detector containing fluorescence telescopes and a ground array of water Cherenkov detection stations [18]. Due to its configuration, it has the capability to observe rare showers induced by neutrinos with energies ranging from 100 PeV to 100 EeV [3, 19]. However, the Pierre

[1]The main mechanism behind neutrino production, the hadronic mechanism, is common to photons

Auger Observatory has not found any neutrino candidates to date, yet it has been capable of imposing stringent constraints on models of neutrino production at EeV energies [20, 21].

The next generation of neutrino detectors is already in development, and includes projects such as SNO+ [9], Hyper-Kamiokande [22], IceCube-Gen2 [23] and KM3-Net [11]. These experiments will build upon previous projects by instrumenting larger volumes and/or employing more advanced neutrino detection technology.

3.2 Ground-Based Gamma-Ray Observatories

The study of extensive air showers generated by VHE gamma- rays falls within the domain of ground-based observatories. These can be divided into two categories [24]: IACT (Imaging Atmospheric Cherenkov Telescopes) such as MAGIC [25], CTA [26], HESS [27] and VERITAS [28], and EAS detector arrays as is the case of HAWC [29], the ARGO-YBJ [30] and LHAASO [31]. The latter category will be complemented by the SWGO [32], which aims to provide coverage of a large portion of the southern sky. Several of these experiments have already been operational for numerous years, resulting in contributions concerning, for example, constraints on Lorentz invariance violation [33], searches for dark matter and its properties [34, 35], and particle acceleration mechanisms in astrophysical objects [36, 37].

4 Implementation

4.1 Shower Generation

The main program used to generate extensive air showers is CORSIKA (COsmic Ray Simulations for KAscade) version 7.7410 [38]. When simulating showers induced by upward-going neutrinos, whose interactions occur in the Earth's crust (a medium which cannot be adequately reproduced using CORSIKA) a different program, AIRES [39] version 2.8.4a, was used.

CORSIKA allows for the specification of several parameters associated with an extensive air shower, such as the primary particle type, its energy, zenith angle (θ), vertical height or vertical depth of the point of the first interaction, the target of this first interaction and the number of showers per run.A few parameters remained unchanged or unaddressed in all simulations, namely: the azimuth angle (ϕ), the magnetic field, and the observation level, which was fixed at 5200m above sea level, corresponding to the altitude of one the sites being considered for SWGO [32].

The signature of a neutrino-induced shower that we aim to investigate is a very inclined shower (θ in the range 60° to 88°) produced close to the ground (vertical height of first interaction up to 12000 m). Thus, very inclined showers induced by neutrinos with energies in the TeV and PeV range are taken as the sources of signal, while background is attributed to very inclined EAS induced by cosmic-rays. For each combination of parameters, 1000 showers were generated, allowing for the creation of S_μ and S_{em} distributions.

AIRES was used for the simulation of showers induced by up-going neutrinos interacting in the Earth's crust close to the detector array. This program does not include neutrinos as a predefined primary particle, so they must be introduced via a so-called special particle file, which is obtained simulating the neutrino interactions through CORSIKA. The neutrino events to be considered are still those associated with very inclined showers, with the distinction that the primary particle is now travelling upwards. The Earth's crust has a much higher density than the atmosphere ($\approx$ 1000 times larger), so showers develop and are attenuated in much shorter lengths. As such, it is only necessary to account for distances of a few meters (up to 5 m) between the point of first interaction and the observation level. The Earth-skimming mechanism associated with up going neutrino events is of particular relevance for the case of VHE and UHE neutrinos, hence the focus of the simulations is set on neutrinos with energies in the PeV range. For each combination of parameters we simulated 1000 showers.

4.2 Detector Response

The amount of signal expected to be registered by a given station of the array when struck by a particle was simulated with Geant4 [40]. The case study used in this work is the SWGO experiment [32], which is expected to rely on water Cherenkov detectors. In these simulations, we'll use one of the candidate configurations for the stations of this observatory [41]. This base unit of the array was represented within Geant4 by a cylindrical tank filled with water, with a base radius of 2 m, height of 1.7 m, and 4 PMTs placed at the bottom, as depicted in Figure 2.

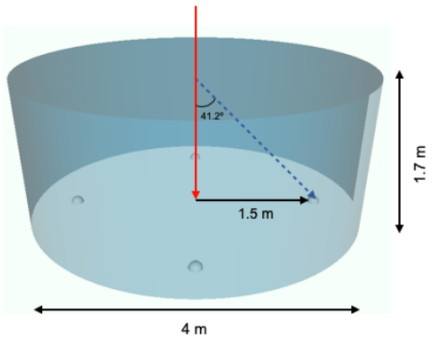

Figure 2: Water Cherenkov detector concept used in this study. The tank is filled with water,and 4 PMTs (Photo Multiplier Tubes) are placed at the bottom of the structure. Taken from [41].

Three types of particles were injected vertically into the station simulation: electrons, muons and protons, to treat the electromagnetic, muonic and hadronic components of an EAS, respectively. For each case, the kinetic energy of the injected particle assumed values ranging from 10 keV to 10 PeV, with 500 particles injected for each combination of energy and primary particle type. These simulations result in the calibration curves presented in Figure 3, which were parameterised to establish

a correspondence between the energy of a particle of an EAS and the signal it generates when it reaches a station of the array. For the purposes of this work, it is sufficient to account only for the average detector response, while neglecting physical fluctuations and other effects, such as clipping particles.

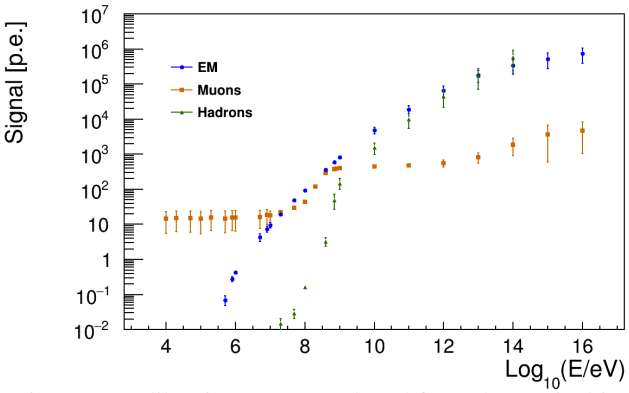

Figure 3: Calibration curve produced from the vertical injection of electrons, muons and protons in the station depicted in Figure 2.

4.3 Shower File Parsing

For the purpose of extracting and saving information pertaining to the shower particles that reach the ground, two C++ codes were created: one to extract information from simulation files generated by CORSIKA, named CORSIKA_explorer, and another to do the same for files generated by AIRES, labelled Aires_reader. The energy, position on the ground, and ID was recorded for each particle. The signal a particle deposited within a station is determined via the previously constructed calibration curves (Figure 3) based on its energy and ID. Summing all EM and muonic signal contributions within an event, we obtain the value of the electromagnetic signal (S_{em}) and muonic signal (S_μ) associated with a given EAS. The full chain of simulation and analysis utilised in this work is summarised in the diagram presented in Figure 4.

5 Results

5.1 Neutrino and Proton-Induced Shower Discrimination

As stated before, the key observables in discriminating between signal events induced by neutrinos and background events generated by cosmic rays are the electromagnetic signal (S_{em}) and muonic signal (S_μ) registered in the simulated WCD stations. This selection of variables is linked to the use of very inclined showers as the signature of neutrino-induced showers. Neutrinos have the possibility of producing showers in close proximity to the detector at steep incidence angles, in which case the electromagnetic component of the resulting showers is more pronounced (a larger S_{em} is produced) in relation to its muonic

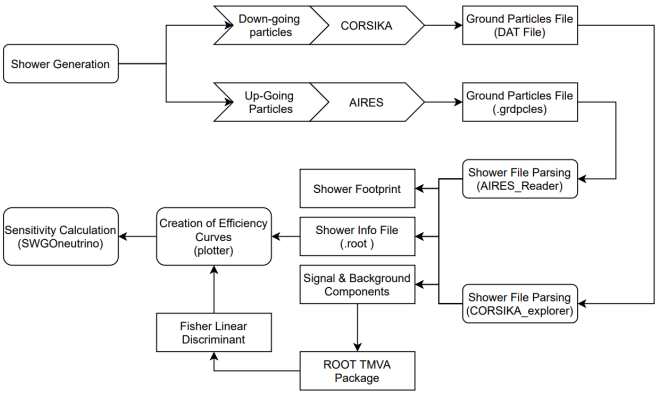

Figure 4: Flow chart depicting the steps, programs, code segments and files involved in the estimation of the sensitivity of an EAS array to neutrinos.

component. In contrast, showers induced by cosmic rays have their first interaction at smaller grammages, thus the ensuing shower is older upon reaching the array, having a more pronounced muonic component (a more significant value of S_μ) in relation to the electromagnetic one. This disparity is the principle we seek to exploit to distinguish signal from background.

Both data pertaining to signal and background is fed into ROOT's Toolkit for Multivariate Data Analysis (TMVA) [42] to separate the two classes of points via a Fisher discriminant, for each fixed zenith angle. Fisher discriminant refers to a group of methods used to find a linear combination of features which separates two or more classes of objects. The result of this analysis may then be used as a linear classifier [43]. Besides this linear cut [2], an additional cut excluding all points with $\log_{10}(S_{em}) > 8.25$ is introduced for the cases with $\theta = 60°$ and $70°$. This cut is added since such high values of electromagnetic signal are unlikely to be achieved by neutrino-induced showers in the energy range below ≈ 10 PeV, which contains most events expected in a detector such as the SWGO. An example containing both kinds of cuts is shown in Figure 5 for the case $\theta = 70°$.

Since the aim is not a good separation between signal and background, but a background free experiment so that any identification would be significant, the value of the normalisation of the Fisher cut is adjusted to the minimum value that achieves this. The efficiency then corresponds to the ratio of neutrino points located below the cut and the total number of neutrino points simulated with a given zenith angle and energy. Applying this procedure to all values of fixed interaction depth of the neutrino-induced showers results in the discrimination efficiency curve of the respective zenith angle, as depicted in Figure 6.

[2] linear cut performed in the space $\log_{10} S_\mu$ vs $\log_{10} S_{em}$

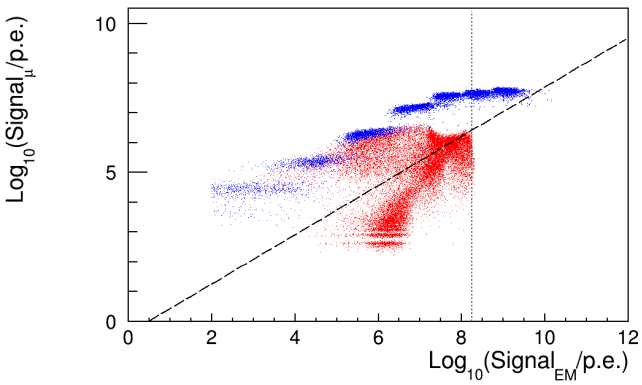

Figure 5: Fisher cut (dashed line) applied in the discrimination between neutrino and proton-induced showers for $\theta = 70°$. Red dots represent neutrino events while blue dots represent proton-induced showers. Dotted line corresponds to the cut in S_{em} above which neutrino-induced showers of energy below $\sim$ 10 PeV are not expected to populate that region of the plot.

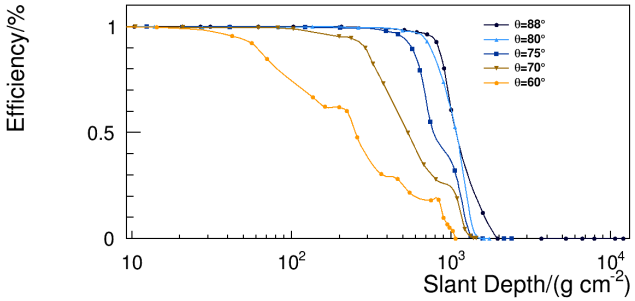

Figure 6: Discrimination efficiency as a function of neutrino interaction slant depth for the cases of showers induced by 1PeV neutrinos, with $\theta = 60°$, 70°, 75°, 80° and 88°.

5.2 Sensitivity of a Ground-Based Gamma-Ray Observatory to Neutrinos

To estimate the sensitivity of a gamma-ray ground-based observatory to neutrinos we have obtained the expected neutrino event rate dN/dt expressed in equation 1.

$$\frac{dN}{dt} = \int_{E_{\nu,min}}^{E_{\nu,max}} \frac{d\Phi(E_\nu)}{dE} \frac{1}{m} \sigma(E_\nu) M_{eff}(E_\nu)\, dE_\nu \quad (1)$$

where $d\Phi/dE$ denotes the differential flux of incoming neutrinos, m is the mass of a nucleon and $\sigma(E_\nu)$ is the neutrino cross section as a function of its energy. Moreover, $M_{eff}(E_\nu)$ is the effective mass associated with a detector as a function of the energy of the incoming neutrino, while E_{max} and E_{min} denote the integration limits used for the sensitivity calculation.

5.2.1 Dependence of Effective Mass on Shower Inclination

The effective mass is defined as the mass within which a neutrino is bound to interact and be identified. The effective mass as a function of the zenith angle (θ) and the energy of the incoming neutrino (E_ν) is expressed in equation 2:

$$\frac{dM_{eff}}{d\theta}(\theta, E_\nu) = \int 2\pi A \sin\theta \cos\theta\, \varepsilon(\theta, D, E_\nu)\, dD \qquad [\mathrm{g}], \quad (2)$$

where $\varepsilon(\theta, D, E_\nu)$ denotes the probability of detecting a neutrino with energy E_ν, injected at a zenith angle θ, and interacting at a slant depth of D. The detection probability is dependent on the cuts introduced to remove the hadronic background. It is a function of the slant depth of the neutrino's point of first interaction D (expressed in g cm^{-2}), the energy of the neutrino E_ν (expressed in GeV) and the angle of incidence θ (expressed in radians). Being an efficiency, it assumes a value between 0 and 1. A is the surface area of the array, initially fixed at a value of 1 km^2.

Starting with 1 PeV showers, five values of θ are considered: 60°, 70°, 75°, 80° and 88°. This wider range of values of θ aims to maximise the resulting neutrino event rate. A cubic spline interpolation is applied to the points of $\varepsilon(\theta, D, E_\nu)$ (E_ν and θ are fixed within each case) in order to integrate in D. This procedure results in the effective mass values reported in Table 1.

Table 1: Effective mass for different values of θ, for neutrino-induced showers with E_ν = 1PeV.

θ	$\frac{dM_{eff}}{d\theta}(\theta, E_\nu = 1\mathrm{PeV})$[g]
60°	9.73×10^{12}
70°	1.27×10^{13}
75°	1.65×10^{13}
80°	9.09×10^{12}
88°	2.21×10^{12}

5.2.2 Total Effective Mass

Making use of the $\frac{dM_{eff}}{d\theta}(\theta, E_\nu)$ values at 1 PeV, equation 2 can be integrated in zenith angle. This calculation is done using equation 3, where zenith angles that were not simulated are obtained via cubic spline interpolation.

$$M_{eff}(E_\nu) = \int \frac{dM_{eff}}{d\theta}(\theta, E_\nu)\, d\theta \qquad [\mathrm{g\ sr}] \quad (3)$$

This integration yields a total effective mass of 2.97×10^{14} g sr, a value that is assumed to remain approximately constant in the 1 – 2 PeV energy bin.

5.2.3 Neutrino Flux

The flux of neutrinos is given by equation 4, where $E_0 = 10^6\,\mathrm{GeV}$, and $k' = kE_0^{-2} = 10^{-20}\,\mathrm{GeV}^{-1}\,\mathrm{cm}^{-2}\,\mathrm{s}^{-1}\,\mathrm{sr}^{-1}$, as extracted from the data made available by the IceCube Neutrino Observatory [44].

$$\frac{d\Phi}{dE}(E_\nu) = k'\left(\frac{E_\nu}{E_0}\right)^{-2} \tag{4}$$

5.2.4 Neutrino Cross Section

The last requirement is the cross section associated with the interaction of incoming neutrinos with the nucleons of the target medium, as a function of their energy. The values required are taken from [45]. The distinction between charged, neutral and total interaction is also made, allowing for the plotting of the 3 curves depicted in Figure 7. The value of neutrino-nucleon interaction cross section for each interaction type can be determined from these plots.

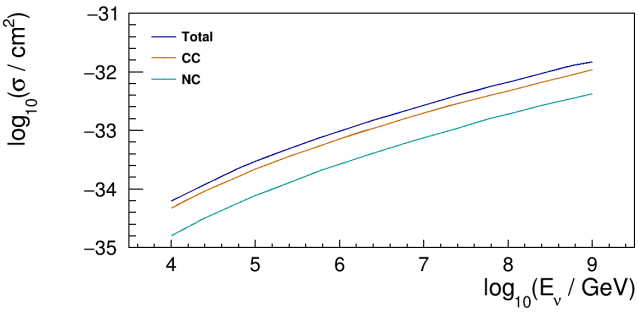

Figure 7: Neutrino-nucleon charged, neutral and total current cross sections. Data taken from [45]

5.2.5 Sensitivity of an EAS observatory to 1 PeV Neutrinos

As all required parameters have been estimated or described as functions of the energy of incoming neutrinos it is possible to compute the sensitivity of a ground-based gamma-ray detector to 1 PeV neutrinos. Replacing the neutrino flux in Eq.2 with Eq.4 results in equation 6.

$$\frac{dN}{dt} = \int_{E_{\nu,min}}^{E_{\nu,max}} k'\left(\frac{E_\nu}{E_0}\right)^{-2}\frac{1}{m}\sigma(E_\nu)M_{eff}(E_\nu)dE_\nu \tag{5}$$

$$= \frac{k'E_0^2\,M_{eff}}{m}\int_{E_{\nu,min}}^{E_{\nu,max}}\frac{\sigma(E_\nu)}{E_\nu^2}dE_\nu \tag{6}$$

Integrating Eq.6 in energy between 1 and 2 PeV yields an event rate of $3.12\times10^{-2}\,\mathrm{yr}^{-1}$, corresponding to roughly one event every 32 years. While this value is far from optimal for an experiment, which typically has a time scale of a few decades, it should be noted that this value was obtained without accounting for the evolution of the effective mass with the energy of the neutrinos. This quantity is expected to increase with energy, as is the number of expected neutrino events. Hence, this evolution shall be discussed in section 5.2.8.

5.2.6 Impact of Neutrino Interaction Channel on Sensitivity

The neutrino detection efficiency and hence the effective mass depend on the interaction channel the neutrino undergoes in order to initiate the cascade. In the previous cases, the interaction channel, either charged current (CC) or neutral current (NC), was randomly chosen according to their relative weight in the total cross section. However, in CORSIKA simulations the type of interactions can be set so that neutrinos only interact via CC or NC, allowing for an alternative approach to the computation of sensitivity where interaction channels are handled individually.

The neutrino detection efficiencies for $E_\nu = 1\,\mathrm{PeV}$ and $\theta = 80°$ are presented in Figure 8, according to the interaction channel selected. Integrating Eq.2 in zenith angle for each case yields the effective mass values reported in Table 2.

Table 2: Values of effective mass for the different neutrino interaction channels CC and NC, with $E_\nu = 1\mathrm{PeV}$. Total corresponds to the case where CC or NC are chosen randomly

Interaction	$M_{eff}(E_\nu = 1\,\mathrm{PeV})[\mathrm{g\,sr}]$
CC	3.60×10^{14}
NC	2.27×10^{14}
Total	2.97×10^{14}

The sum of the effective masses obtained for NC and CC individually, $5.87\times10^{14}\,\mathrm{g\,sr}$, is larger than the effective mass associated with a random type of interaction, $2.97\times10^{14}\,\mathrm{g\,sr}$. To determine whether this distinction is beneficial, the interaction cross section must also be accounted for, as given by the curves in Figure 7. The other remaining factor, the neutrino flux, has no dependence on the type of interaction.

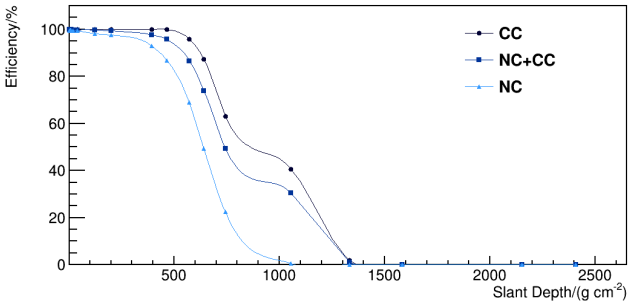

Figure 8: Discrimination efficiency curves obtained for showers induced by 1 PeV neutrinos with $\theta = 75°$. Interactions are either selected at random according to their cross sections (NC+CC), or set explicitly to only charged (CC) or neutral current (NC) interactions.

Employing the effective masses listed in Table 2, Eq.6 is integrated in energy for the cases where interactions occurs via NC or CC, yielding the rates listed in Table

3. The event rate obtained for a random interaction type, $3.12 \times 10^{-2}\,\mathrm{yr}^{-1}$, exceeds the sum of the individual cases where the first interaction occurs either exclusively via CC or NC, $2.54 \times 10^{-2}\,\mathrm{yr}^{-1}$. Thus, the approach in which CC or NC are chosen according to their relative cross sections maximises the number of expected events per year.

Table 3: Sensitivity of a wide-field ground-based gamma-ray observatory to astrophysical neutrinos, according to the type of the first interaction. E_ν spanning from 1PeV to 2 PeV

Interaction	$\frac{dN}{dt}[\mathrm{yr}^{-1}]$
CC	2.29×10^{-2}
NC	2.50×10^{-3}
Total	3.12×10^{-2}

5.2.7 *Sensitivity to* 100 TeV *Neutrinos*

A study was also carried out for neutrinos with E_ν = 100 TeV, where energy spectrum is dominated by the atmospheric neutrino flux. A procedure identical to the one described in sections 5.2.1 - 5.2.5 was followed. This computation took into consideration 3 values of zenith angle $\theta = 75°$, 80° and 88°, instead of the previous 5 values, as such a selection did not result in a significant increase of the expected event rate for E_ν = 1PeV. The resulting efficiency curves are depicted in Figure 9, and are employed in the procedure described in section 5.2.1 to obtain the effective mass for the 3 values of zenith angle, as listed in Table 4.

Table 4: Effective mass for different values of θ for neutrino-induced showers, with E_ν = 100TeV.

θ	$\frac{dM_{eff}}{d\theta}(\theta, E_\nu = 100\mathrm{TeV})[\mathrm{g}]$
75°	1.16×10^{13}
80°	8.47×10^{12}
88°	2.18×10^{12}

Taking into account the $M_{eff}(\theta, E_\nu)$ values at 100 TeV, equation 2 is integrated in zenith angle. Following the procedure described in section 5.2.2, the resulting total effective mass is 9.55×10^{13} g sr, and is assumed to remain constant in the 100 − 200 TeV energy bin.The neutrino flux is given by Eq.4 and the cross section is determined via the plots presented in Figure 7. Integrating Eq.6 over the neutrino energy (E_ν spanning from 100TeV to 200 TeV) yields an event rate of $3.14 \times 10^{-2}\,\mathrm{yr}^{-1}$, corresponding to approximately one event every 32 years, as was the case for E_ν = 1 PeV.

5.2.8 *Evolution of the Effective Mass with the Primary Energy*

It is possible to attempt to find a function to describe the growth of the effective mass with neutrino energy. The

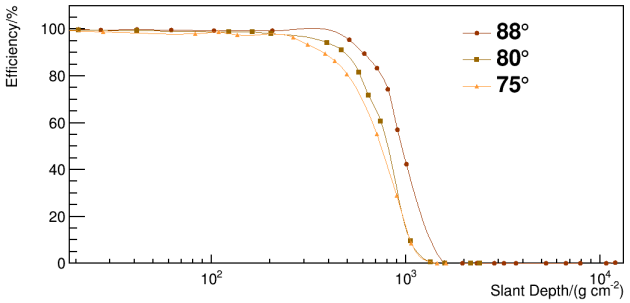

Figure 9: Discrimination efficiency curves obtained for the cases of showers induced by 100TeV neutrinos, with θ = 75°, 80° and 88°.

effective mass is approximately proportional to the neutrino cross section, that grows linearly with energy for energies below 100 TeV, and as the energy increases its dependence shifts towards $E_\nu^{1/3}$. As such, a power law was fitted to the two values of total effective mass calculated, and the growth of effective mass with the neutrino energy was described with Eq.7. As there are no simulations above 1 PeV, the extrapolation towards higher energies is more uncertain. To estimate the impact of such uncertainty on the effective mass calculation, an optimistic solution ($M_{eff} \propto E_\nu$) and a pessimistic one ($M_{eff} \propto E_\nu^{1/3}$) are considered.

$$M_{eff} = \left(2.97454 \times 10^{14}\right) \times \left(\frac{E}{1\,\mathrm{PeV}}\right)^{0.5} \quad [\mathrm{g\,sr}] \qquad (7)$$

The event rate is given by Eq.8, as the function used to describe effective mass has an explicit dependence on energy.

$$\frac{dN}{dt} = \frac{k' E_0^2}{m} \int_{E_{\nu,min}}^{E_{\nu,max}} \frac{\sigma(E_\nu)\, M_{eff}(E_\nu)}{E_\nu^2} dE_\nu \qquad (8)$$

Using Eq.8 to estimate the event rate for the cases discussed in sections 5.2.5 and 5.2.7 yields the values reported in Table 5 and 6, respectively.

Table 5: Sensitivity of a wide-field ground-based gamma-ray observatory (A = 1 km^2) to 1 PeV neutrinos, according to the function used to describe $M_{eff}(E_\nu)$.E_ν spanning from 1PeV to 2 PeV

Model of $M_{eff}(E_\nu)$	$\frac{dN}{dt}[\mathrm{yr}^{-1}]$
Constant	3.12×10^{-2}
Linear	4.09×10^{-2}
$\propto E_\nu^{0.5}$	3.70×10^{-2}
$\propto E_\nu^{1/3}$	3.58×10^{-2}

For E_ν spanning from 1PeV to 2 PeV, the $M_{eff} \propto E^{0.5}$ model estimates an event every 27 years, while the case with $M_{eff} \propto E^{1/3}$ points to an event every 25 years. For E_ν spanning from 100TeV to 200 TeV, the $M_{eff} \propto E^{0.5}$ model also indicates an event every 27 years, while the

Table 6: Sensitivity of a wide-field ground-based gamma-ray observatory ($A = 1\,\mathrm{km}^2$) to 100 TeV neutrinos, according to the function used to describe $M_{eff}(E_\nu)$.E_ν spanning from 100TeV to 200 TeV

Model of $M_{eff}(E_\nu)$	$\frac{dN}{dt}[\mathrm{yr}^{-1}]$
Constant	3.14×10^{-2}
Linear	3.45×10^{-2}
$\propto E_\nu^{0.5}$	3.67×10^{-2}
$\propto E_\nu^{1/3}$	3.82×10^{-2}

$M_{eff} \propto E^{1/3}$ solution estimates an event every 29 years. Both the $M_{eff} \propto E^{1/3}$ and $M_{eff} \propto E^{0.5}$ approaches result in an increase of the expected event rate, when compared to the case where the total effective mass remains constant.

5.2.9 *Measured Integral Neutrino Flux*

5.2.10 PeV *Neutrinos*

The estimate of sensitivity can be extended to larger values of the upper energy integration limit and the area of the detector. A more realistic maximum energy value of 10 PeV is introduced, followed by an extrapolated case with an upper limit of 100 PeV, where the flux of astrophysical neutrinos is unknown. Similarly, values of the area of the detector range from $5 \times 10^4 \mathrm{m}^2$ to $10^7 \mathrm{m}^2 (10\,\mathrm{km}^2)$. The results of these two considerations, assuming $M_{eff} \propto E^{0.5}$ as described by Eq.7, are presented in Figure 10.

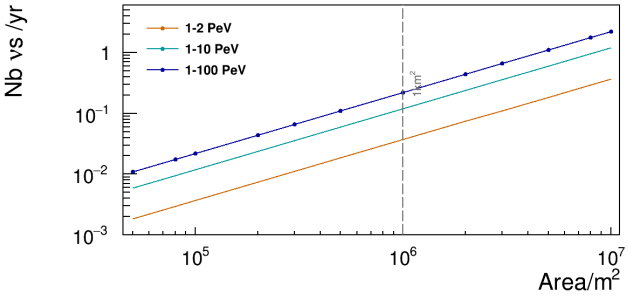

Figure 10: Number of astrophysical neutrinos expected to be detected and identified per year, as a function of the area of the detector. 3 curves are presented corresponding to different ranges of energies used during the sensitivity computation. At the time of writing, the SWGO is projected to have an area of $1\mathrm{km}^2$, which is indicated by a dashed vertical line. The model in which $M_{eff} \sim E_\nu^{0.5}$ is adopted.

To evaluate the impact of the choice of function used to describe the effective mass with energy, we consider the scenarios where the effective mass is constant, proportional to the energy or where it follows a power law of the kind $\propto E^{1/3}$ or $\propto E^{0.5}$. Under these conditions, the results listed in Tables 7 and 8 are obtained.

Table 7: Sensitivity of a wide-field ground-based gamma-ray observatory ($A = 1\,\mathrm{km}^2$) to astrophysical neutrinos, for each model of $M_{eff}(E_\nu)$ .E_ν spanning from 1PeV to 10 PeV.

Model of $M_{eff}(E_\nu)$	$\frac{dN}{dt}(E_{\nu_{max}} = 10\,\mathrm{PeV})[\mathrm{yr}^{-1}]$
Constant	7.12×10^{-2}
Linear	1.83×10^{-1}
$\propto \mathbf{E_\nu^{0.5}}$	$\mathbf{1.19 \times 10^{-1}}$
$\propto E_\nu^{1/3}$	1.06×10^{-1}

Table 8: Sensitivity of a wide-field ground-based gamma-ray observatory ($A = 1\,\mathrm{km}^2$) to astrophysical neutrinos, for each model of $M_{eff}(E_\nu)$ .E_ν spanning from 1PeV to 100 PeV

Model of $M_{eff}(E_\nu)$	$\frac{dN}{dt}(E_{\nu_{max}} = 100\,\mathrm{PeV})[\mathrm{yr}^{-1}]$
Constant	9.26×10^{-2}
Linear	6.21×10^{-1}
$\propto \mathbf{E_\nu^{0.5}}$	$\mathbf{2.20 \times 10^{-1}}$
$\propto E_\nu^{1/3}$	1.72×10^{-1}

Excluding the model with constant effective mass, the most conservative sensitivity estimates in both Table 7 and 8 are obtained when the effective mass is assumed to follow a $\propto E^{1/3}$ power law, whereas the largest value is obtained when employing a linear model. This behaviour is dominant for energies below 100 TeV, a value which is at the bottom edge of the currently considered range of energies. Given these observations and the limited amount of data available, the most reasonable approach is the one where the effective mass follows a power law according to $E_\nu^{0.5}$. For E_ν spanning from 1PeV to 10 PeV and to 100 PeV this model estimates an event every ~ 9 and ~ 4 years, respectively.

5.2.11 100 TeV *Neutrinos*

The procedure followed in the previous section is now applied to the study of $E_\nu = 100$ TeV. Besides the case with 100 – 200 TeV, two additional possibilities are considered: from 100 TeV to 1 PeV, and from 100 TeV to 100 PeV. The latter case aims to encompass all possible VHE neutrino events. Plotting these three cases as functions of the detector's surface area results in the curves depicted in Figure 11.

The impact of the choice of the description of effective mass as a function of energy is once again evaluated. Accounting for the same possibilities listed in the previous section, the resulting event rates are reported in Tables 9 and 10.

The results listed in Tables 9 and 10 follow a pattern different from that present in Tables 7 and 8. The most conservative sensitivity estimate is associated with a constant effective mass, while the largest value is obtained when the effective mass is assumed to grow linearly with

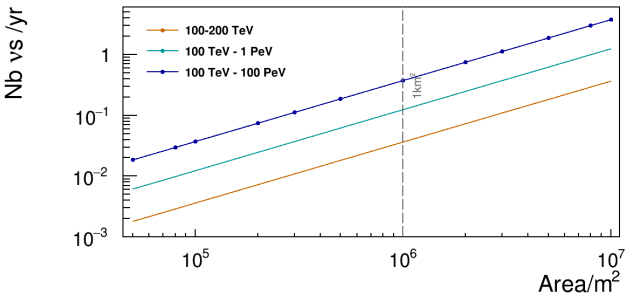

Figure 11: Number of atmospheric neutrinos expected to reach the detector per year, as a function of its area. 3 curves are presented corresponding to different ranges of energies used during the sensitivity calculation. At the time of writing, the detector is projected to have an area of 1km^2, which is indicated by a dashed vertical line. A model in which $M_{eff} \sim E_\nu^{0.5}$ is adopted.

Table 9: Sensitivity of a wide-field ground-based gamma-ray observatory ($A = 1\,\mathrm{km}^2$) to atmospheric neutrinos, for each $M_{eff}(E_\nu)$ model. E_ν spanning from 100TeV to 1 PeV.

Model of $M_{eff}(E_\nu)$	$\frac{dN}{dt}(E_{\nu_{max}} = 1\,\mathrm{PeV})[\mathrm{yr}^{-1}]$
Constant	8.50×10^{-2}
Linear	1.13×10^{-1}
$\propto \mathbf{E_\nu^{0.5}}$	$\mathbf{1.25 \times 10^{-1}}$
$\propto E_\nu^{1/3}$	1.30×10^{-1}

Table 10: Sensitivity of a wide-field ground-based gamma-ray observatory ($A = 1\,\mathrm{km}^2$) to neutrinos, for each $M_{eff}(E_\nu)$ model.E_ν spanning from 100TeV to 100 PeV.

Model of $M_{eff}(E_\nu)$	$\frac{dN}{dt}(E_{\nu_{max}} = 100\,\mathrm{PeV})[\mathrm{yr}^{-1}]$
Constant	1.37×10^{-1}
Linear	7.64×10^{-1}
$\propto \mathbf{E_\nu^{0.5}}$	$\mathbf{3.72 \times 10^{-1}}$
$\propto E_\nu^{1/3}$	3.01×10^{-1}

energy for $E_{\nu_{max}} = 100\,\mathrm{PeV}$, and when it follows a $E_\nu^{1/3}$ power law for $E_{\nu_{max}} = 1\,\mathrm{PeV}$. The description where effective mass follows a power law according to $E_\nu^{0.5}$ leads to an estimation of one event every ~ 8 and ~ 3 years for E_ν spanning from 100TeV to 1 PeV and to 100 PeV, respectively.

5.3 Impact of Experimental Signal Resolution on Sensitivity

A study of the impact of experimental resolution in the expected event rates was also carried out, by applying a Gaussian smearing to both electromagnetic and muonic signals, of both signal and background events. Denoting the fluctuations applied to the electromagnetic signal as $\sigma_{S_{em}}$ and to the muonic signal as σ_{S_μ}, the smearing is applied according to a Gaussian distribution, whose mean value is the unmodified signal as expressed by Eq. 9.

$$f_{S_{em}}(x) = \frac{1}{\sigma_{S_{em}}\sqrt{2\pi}} e^{-\frac{1}{2}\left(\frac{x-S_{em}}{\sigma_{S_{em}}}\right)}, \quad f_{S_\mu}(x) = \frac{1}{\sigma_{S_\mu}\sqrt{2\pi}} e^{-\frac{1}{2}\left(\frac{x-S_\mu}{\sigma_{S_\mu}}\right)} \tag{9}$$

Making use of this formulation, fluctuations ranging from 0 to 50% were introduced for both electromagnetic and muonic signal. Since the fluctuations are applied to both signal and background events, the offset of the associated cuts must be readjusted accordingly, to ensure that background is still completely eliminated. The result of smearing being applied to the detection of astrophysical neutrinos with energies ranging from 1 PeV to 10 PeV is presented in Figure 12, assuming a surface area of 1 km^2. Larger values of either σ_{S_μ} or $\sigma_{S_{em}}$ result in progressively lower event rates and hence lower sensitivity, as would be expected.

To further explore the impact of signal fluctuations, the same smearing procedure was applied to a wider range of $\sigma_{S_{em}}$ and σ_{S_μ}, reaching a maximum value of 500%. This results in the graph presented in Figure 13, where it can be seen that a degradation of the expected number of neutrinos by a factor of 2 is only reached when the smear applied to either the electromagnetic or muonic signal reaches values nearing 200%. This small impact of the signal degradation is a consequence of the cuts being applied to the logarithm of these two variables.

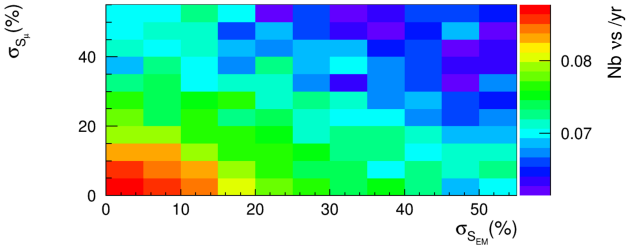

Figure 12: Neutrino event rate as a function of the σ of the Gaussian smearing applied to the electromagnetic and muonic signal. Calculations performed for the range of energies 1 PeV – 10 PeV, assuming the detector's surface area is 1 km^2. The model of $M_{eff} \sim E_\nu^{0.5}$ has been adopted.

5.4 Up-Going Neutrinos

The final case is that of up-going earth-skimming neutrinos interacting underground in close proximity to the detector array (less than 5 m vertically). Using the AIRES (more specifically, ZHAIRES) framework, it is possible to set the composition of the atmosphere to match that of standard soil as taken from [46]: $\rho = 1.8\,\mathrm{g\,cm}^{-3}$ and effective $Z = 11$.

The framework was utilised to simulate showers generated by up-going neutrinos with an energy of 1 PeV, inclinations ranging from $\theta = 60°$ to $88°$, and made to interact at fixed vertical heights of 2 m, 3 m and 5 m below the observation level.From this procedure, it was possible to

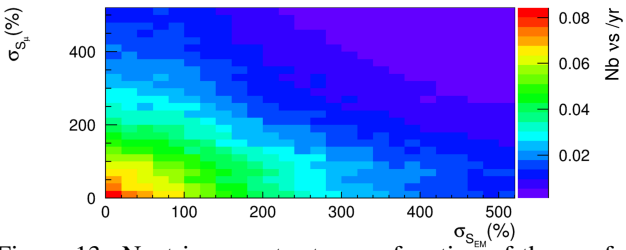

Figure 13: Neutrino event rate as a function of the σ of the Gaussian smearing applied to the electromagnetic and muonic signal, up to 500%. Calculations performed for the range of energies 1 PeV – 10 PeV, assuming the detector's surface area is 1 km^2. The model of $M_{eff} \sim E_\nu^{0.5}$ has been adopted.

infer the average footprints produced in each case (an example is presented in Figures 14), and determine whether an observatory such as the SWGO would be capable of discerning these events.

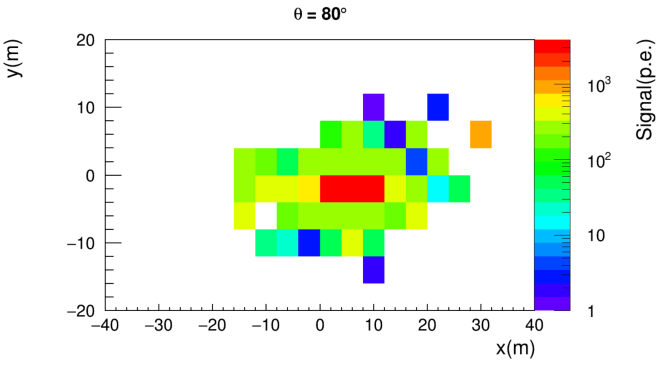

Figure 14: Average footprint produced by a shower induced by an up-going neutrino with $E_\nu = 1$ PeV and $\theta = 80°$ interacting at a vertical height of 3 m below the observation level.

Given the shape and small dimensions of these footprints (of the order of a few tens of m^2), the observatory cannot reliably detect showers generated by up-going neutrinos, since there would not be enough individual detectors triggered. This is more so the case if these showers reached only the sparse array of the observatory, where the interval between neighbouring stations is approximately 20 m. For these reasons, showers induced by up-going neutrinos were discarded in the estimation of the sensitivity of an EAS array to neutrinos.

5.5 Summary

In this thesis we carried out a study of the sensitivity of a km^2-scale wide-field ground-based gamma-ray observatory to VHE atmospheric and astrophysical neutrinos. Taking into account the results pertaining to down-going neutrinos, it is reasonable to state that such an observatory is predicted to be capable of detecting both classes of neutrinos in a decade-long observation, with a high cosmic-ray background reduction.Overall, the sensitivity obtained for both astrophysical and atmospheric neutrinos bears a noticeable degree of similarity, as they exhibit comparable discrimination efficiency curves (in the zenith angle range common to both cases), and the resulting expected event rates differ by less than 1% from one another (when comparing the case of 1 – 2 PeV and 100 – 200 TeV with $M_{eff} \sim E_\nu^{0.5}$).

On a separate note, we studied the relative contribution of the CC and NC interaction channels to the expected astrophysical neutrino event rate. The dominating contribution in effective mass was associated with CC interactions. However, when accounting for the cross section of each interaction channel, the adoption of a more a realistic approach in which CC or NC are chosen according to their relative cross sections proved most beneficial.

We also studied the effect on the event rates of the choice of the model describing the growth of the total effective mass with the neutrino energy. When this quantity was assumed to remain constant within small energy bins, the resulting sensitivity was underestimated, such that collecting ~ 1 neutrino event would require a time scale comparable to or even exceeding that of a typical experiment, thus emphasising the need to account for the evolution of the total effective mass with energy. Given the importance of this factor, two limiting cases were considered: an optimistic one where the total effective mass was assumed to evolve linearly with energy, and a pessimistic one that assumes that the total effective mass grows with $E_\nu^{1/3}$. It became clear that additional shower simulations at around $E_\nu = 10$ PeV would be important in avoiding extrapolation towards higher energies. This will be addressed in the future. Ultimately, the approach deemed most reasonable was the $M_{eff} \sim E_\nu^{0.5}$ power law. This function represents a halfway point between the optimistic behaviour associated with lower energies ($E_\nu < 100$ TeV) and the pessimistic one expected at higher energies ($E_\nu > 1$ PeV).

Regarding the impact of the experimental resolution, it was noted that a degradation of the expected neutrino event rate by a factor of 2 would require extreme resolutions of the order of 200% for either the electromagnetic or muonic signal. Thus, experimental resolution does not appear to pose a decisive obstacle in the detection of neutrinos by ground-based gamma-ray observatories, under the conditions established in the present thesis.

Based on the results obtained from the injection of up-going neutrinos, it is clear these events do not contribute to the sensitivity of the gamma-ray observatory. This is due to the small dimensions of the footprints produced in these events, which would require a higher density of stations in the sparse array to allow for a proper detection of incoming particles. It must be noted this work did not evaluate additional possibilities that would increase the neutrino event rate, such as neutrinos interacting within geological formations, namely mountains, as this would largely depend on the topology of the site of the experiment in question. Incorporating tau neutrinos into this calculation would further increase this number. Therefore, the expected event rates reached in this thesis represent only a lower bound of the possibility of neutrino detection using an EAS array and serve to accentuate the viability of this measurement.

References

[1] U. Katz, C. Spiering, Progress in Particle and Nuclear Physics **67**, 651–704 (2012)

[2] L. Lu, T. Yuan, Nuclear Instruments and Methods in Physics Research Section A: Accelerators, Spectrometers, Detectors and Associated Equipment **970**, 163678 (2020), a RICH LEGACY

[3] P.Billoir, O.B.Bigas, Nuclear Physics B - Proceedings Supplements **168**, 225 (2007), proceedings of the Neutrino Oscillation Workshop

[4] A. Aab et al., The Astrophysical Journal **902**, 105 (2020)

[5] C. Aramo et al., Astroparticle Physics **23**, 65–77 (2005)

[6] I. Belolaptikov et al., Astroparticle Physics **7**, 263 (1997)

[7] M.G. Aartsen et al., Journal of Instrumentation **arXiv:1612.05093** (2016)

[8] A. Bellerive et al., Nuclear Physics B **908**, 30–51 (2016)

[9] V. Albanese et al., Journal of Instrumentation **16**, P08059 (2021)

[10] S. Fukuda et al., Nuclear Instruments and Methods in Physics Research Section A: Accelerators, Spectrometers, Detectors and Associated Equipment **501**, 418 (2003)

[11] J. Hernández Rey et al., Journal of Instrumentation **16**, C09016 (2021)

[12] F. Reines, C. Cowan, Phys. Rev. **92**, 830 (1953)

[13] K. Eguchi et al. (KamLAND Collaboration), Phys. Rev. Lett. **90**, 021802 (2003)

[14] V. Gavin, Phys. Atom. Nuclei **76**, 1238 (2013)

[15] F. Kaether et al., Physics Letters B **685**, 47–54 (2010)

[16] I. Collaboration, Science **342** (2013)

[17] I. Collaboration, Science **361** (2018)

[18] P.A. Collaboration, Nuclear Instruments and Methods in Physics Research Section A: Accelerators, Spectrometers, Detectors and Associated Equipment **798**, 172–213 (2015)

[19] S. Pastor, Nuclear Physics B - Proceedings Supplements **235-236**, 358 (2013), the XXV International Conference on Neutrino Physics and Astrophysics

[20] A.Aab, P.Abreu, M.Aglietta, et al., The Astrophysical Journal **902**, 105 (2020)

[21] A.Aab, P.Abreu, M.Aglietta, et al., Journal of Cosmology and Astroparticle Physics **2019**, 022–022 (2019)

[22] H.K. Proto-Collaboration, K. Abe et al., *Hyper-kamiokande design report* (2018), 1805.04163

[23] G. Collaboration, M. Aartsen et al., *Icecube-gen2: A vision for the future of neutrino astronomy in antarctica* (2014), 1412.5106

[24] F. Aharonian et al., Rep. Prog. Phys **71**, 96901 (2008)

[25] D. Bastieri et al., Frontiers of Fundamental Physics p. 291–296 (2006)

[26] (2018)

[27] D. Gottschall et al., *The mirror alignment and control system for ct5 of the h.e.s.s. experiment* (2015), 1509.04100

[28] N. Park, *Performance of the veritas experiment* (2015), 1508.07070

[29] H. Vargas, *Prospects of earth-skimming neutrino detection with hawc* (2019), 1908.07622

[30] G. Sciascio, *Highlights from the argo-ybj experiment* (2010), 1012.4400

[31] X. Bai et al., *The large high altitude air shower observatory (lhaaso) science white paper* (2019), 1905.02773

[32] P. Abreu et al., *The southern wide-field gamma-ray observatory (swgo): A next-generation ground-based survey instrument for vhe gamma-ray astronomy* (2019), 1907.07737

[33] B. Zitzer, *Lorentz invariance violation limits from the crab pulsar using VERITAS* (2013), 1307.8382

[34] M. Pierre, J. Siegal-Gaskins, P. Scott, Journal of Cosmology and Astroparticle Physics **2014**, 024–024 (2014)

[35] J. Aleksić et al., Journal of Cosmology and Astroparticle Physics **2011**, 035–035 (2011)

[36] S. Marinelli, J. Goodman, *Measuring high-energy spectra with HAWC* (2017), 1708.03502

[37] M. Balbo, R. Walter, *Gamma-rays and positrons from colliding wind binaries* (2019), 1909.00793

[38] D. Heck, J.N. Capdevielle, G. Schatz, T. Thouw, F.K. Gmbh, *Corsika: A monte carlo code to simulate extensive air showers," report fzka 6019, forschungszentrum karlsruhe* (1998)

[39] S.J. Sciutto (1999), astro-ph/9911331

[40] S. Agostinelli et al., Nucl. Instrum. Meth. **A506**, 250 (2003)

[41] R. Conceição et al., Eur. Phys. J. C **81**, 542 (2021), 2101.10109

[42] A. Hoecker, P. Speckmayer, J. Stelzer, J. Therhaag, E. Toerne, H. Voss, M. Backes, T. Carli, O. Cohen, A. Christov et al., *TMVA - Toolkit for Multivariate Data Analysis* (2007)

[43] R.A. Fisher, Annals of Eugenics **7**, 179 (1936)

[44] R. Abbasi et al. (IceCube Collaboration), Phys. Rev. D **104**, 022002 (2021)

[45] A. Connolly, R.S. Thorne, D. Waters, Physical Review D **83**, 113009 (2011)

[46] M. Tueros, S. Sciutto, Computer Physics Communications **181**, 380 (2010)